Inorganic Chemistry

Article

pubs.acs.org/IC

Topochemical Fluorination of $Sr_3(M_{0.5}Ru_{0.5})_2O_7$ (M = Ti, Mn, Fe), n = 2, Ruddlesden–Popper Phases

Fabio Denis Romero,[†] Paul A. Bingham,[‡] Susan D. Forder,[‡] and Michael A. Hayward*[,†]

[†]Department of Chemistry, University of Oxford, Inorganic Chemistry Laboratory, South Parks Road, Oxford, OX1 3QR, United Kingdom

[‡]Materials and Engineering Research Institute, Sheffield Hallam University, City Campus, Howard Street, Sheffield, S1 1WB, United Kingdom

Supporting Information

ABSTRACT: Reaction of the appropriate $Sr_3(M_{0.5}Ru_{0.5})_2O_7$ (M = Ti, Mn, Fe), n = 2, Ruddlesden–Popper oxide with CuF_2 under flowing oxygen results in formation of the oxide–fluoride phases $Sr_3(Ti_{0.5}Ru_{0.5})_2O_7F_2$, $Sr_3(Mn_{0.5}Ru_{0.5})_2O_7F_2$, and $Sr_3(Fe_{0.5}Ru_{0.5})_2O_{5.5}F_{3.5}$ via a topochemical anion insertion/substitution process. Analysis indicates the titanium and manganese phases have Ti^{4+}, Ru^{6+} and Mn^{4+}, Ru^{6+} oxidation state combinations, respectively, while Mössbauer spectra indicate an Fe^{3+}, $Ru^{5.5+}$ combination for the iron phase. Thus, it can be seen that the soft fluorination conditions employed lead to formation of highly oxidized Ru^{6+} centers in all three oxide–fluoride phases, while oxidation states of the other transition metal M cations remain unchanged. Fluorination of $Sr_3(Ti_{0.5}Ru_{0.5})_2O_7$ to $Sr_3(Ti_{0.5}Ru_{0.5})_2O_7F_2$ leads to suppression of magnetic order as the fluorinated material approaches metallic behavior. In contrast, fluorination of $Sr_3(Mn_{0.5}Ru_{0.5})_2O_7$ and $Sr_3(Fe_{0.5}Ru_{0.5})_2O_7$ lifts the magnetic frustration present in the oxide phases, resulting in observation of long-range antiferromagnetic order at low temperature in $Sr_3(Mn_{0.5}Ru_{0.5})_2O_7F_2$ and $Sr_3(Fe_{0.5}Ru_{0.5})_2O_{5.5}F_{3.5}$. The influence of the topochemical fluorination on the magnetic behavior of the $Sr_3(M_{0.5}Ru_{0.5})_2O_xF_y$ phases is discussed on the basis of changes to the ruthenium oxidation state and structural distortions.

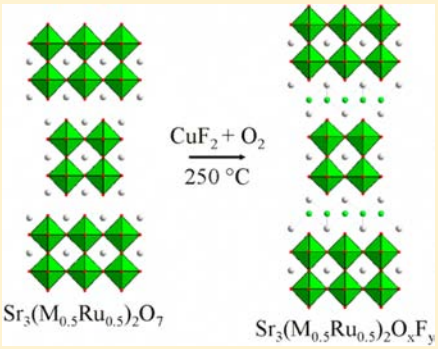

INTRODUCTION

Complex transition metal oxides have been the subject of widespread study due to the diverse array of electronic and magnetic behaviors they exhibit. These complex and often useful properties can be attributed to the presence of electrons in partially filled metal d states which couple to each other though exchange and other orbital interactions that are often mediated by the surrounding anion lattice. Thus, the physical behavior of complex transition metal oxides can be considered to be the product of both the transition metal d-electron count (metal oxidation states) and the extended structure of the oxide phase.[1,2]

The refractory nature of most binary metal oxides means that the majority of complex oxide phases need to be prepared at high temperature. Under such conditions the structures and compositions of product phases are determined by thermodynamic considerations—the most thermodynamically stable phase or mixture of phases being prepared. This necessarily limits the variety of structure types and metal oxidation states which can be adopted by materials prepared by this route to a small set of thermodynamically stable combinations. Low-temperature topochemical synthesis routes enable a degree of kinetic control to be applied to product selection, and as a result they allow preparation of metastable phases with novel combinations of oxidation state and extended structure. Thus, for example, by performing low-temperature anion deintercalation reactions on suitable host materials, extended oxide phases containing Ni^{1+}, Co^{1+}, or even Mn^{1+} can be prepared with structures based on perovskite-type cation lattices.[3−5]

To complement the preparation of novel reduced phases by such anion deintercalation reactions, a range of low-temperature topochemical oxidation reactions have also been developed to prepare metastable phases with highly oxidized transition metal centers via insertion of additional anions, typically oxide or fluoride ions, into extended transition metal oxide hosts.[6−8] In order for these reactions to proceed effectively, the host phase must contain not only oxidizable transition metal centers but also suitable intercalation sites to accommodate the inserted species.

$(AO)(ABO_3)_n$ Ruddlesden–Popper phases, which consist of a regular stacking of AO 'rock salt' layers and ABO_3 perovskite blocks n octahedra thick, contain suitable tetrahedral anion insertion sites within the rock salt layers. These sites allow topochemical insertion of anions into phases with this structure type to yield oxidized metastable materials,[10−17] as exemplified by fluorination of the n = 2 Ruddlesden–Popper phase $Sr_3Ru_2O_7$ to $Sr_3Ru_2O_7F_2$, as shown in Figure 1.[9] A rather unusual feature of reactions of this type is that the additional anions are inserted into locations within the host structure

Received: January 17, 2013
Published: February 26, 2013

   dx.doi.org/10.1021/ic400125x | Inorg. Chem. 2013, 52, 3388−3398

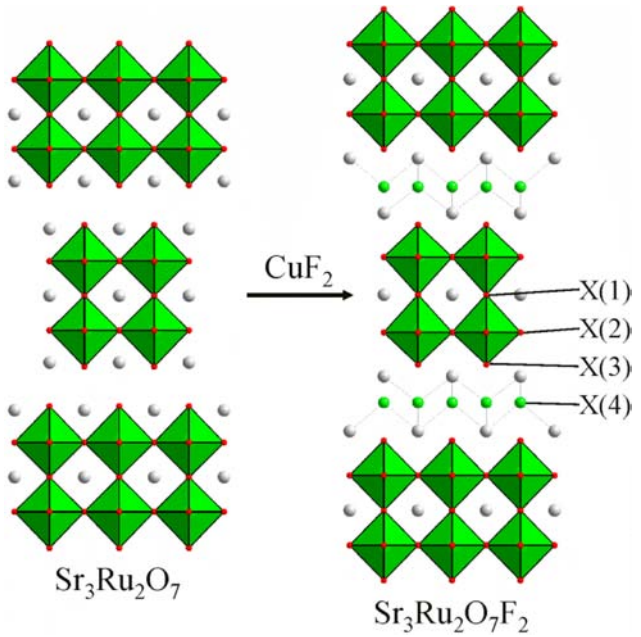

Figure 1. Schematic of the topochemical fluorination of $Sr_3Ru_2O_7$ to $Sr_3Ru_2O_7F_2$.[9] Fluoride ions are inserted into tetrahedral interstitial sites which lie at the interface of the rock salt and perovskite blocks (X(4)) within the Ruddlesden–Popper host structure.

which are remote from the transition metal center being oxidized. As a result the oxidation states of the transition metal centers are changed (raised) while their local coordination spheres, and thus their relative d-orbital energies, remain largely unchanged. Therefore, these remote anion insertions into the rock salt layers of Ruddlesden–Popper phases can be thought of as almost pure electronic doping processes.

Here we describe the topochemical fluorination of a number of mixed cation $Sr_3(M_{0.5}Ru_{0.5})_2O_7$, $n = 2$, Ruddlesden–Popper phases in order to study the magnetic and physical properties of the resulting metastable materials.

EXPERIMENTAL SECTION

Synthesis of $Sr_3(M_{0.5}Ru_{0.5})_2O_7$ (M = Fe, Mn). Samples of $Sr_3(Fe_{0.5}Ru_{0.5})_2O_7$ and $Sr_3(Mn_{0.5}Ru_{0.5})_2O_7$ were prepared using a citrate gel synthesis method. Suitable quantities of $SrCO_3$ (99.99%), RuO_2 (99.99%, dried at 800 °C for 2 h), and Fe_2O_3 (99.99%) or MnO_2 (99.997%) were dissolved in a minimum quantity of a 1:1 mixture of 6 M nitric acid and distilled water. A 3.33 mol equiv of citric acid and 5 mL of analar ethylene glycol were added, and the solution was heated with constant stirring. Gels thus formed were subsequently ground into fine powders, placed in alumina crucibles, and heated at 1 °C min^{-1} to 1000 °C in air to remove the remaining organic components. The resulting powders were pressed into 13 mm diameter pellets and heated as described previously by Battle et al.:[18,19] samples of $Sr_3(Fe_{0.5}Ru_{0.5})_2O_7$ were heated at 1200 °C for 2 days followed by 1300 °C for 4 days with intermediate regrinding and repelletizing; samples of $Sr_3(Mn_{0.5}Ru_{0.5})_2O_7$ were heated at 1400 °C for 2 periods of 4 days with intermediate grinding and pelletizing. Resulting materials were observed to be phase pure by laboratory X-ray powder diffraction, with lattice parameters $a = 3.917(1)$ Å, $c = 20.396(2)$ Å and $a = 3.905(1)$ Å, $c = 20.140(2)$ Å for $Sr_3(Fe_{0.5}Ru_{0.5})_2O_7$ and $Sr_3(Mn_{0.5}Ru_{0.5})_2O_7$, respectively, in good agreement with literature values.[18,19]

Synthesis of $Sr_3(Ti_{0.5}Ru_{0.5})O_7$. Samples of $Sr_3(Ti_{0.5}Ru_{0.5})O_7$ were prepared via a ceramic route. Suitable quantities of $SrCO_3$, RuO_2, and TiO_2 (99.995%) were ground together in an agate mortar and pestle and then heated in air at 1000 °C to decompose the carbonate. Resulting material was then reground, pressed into 13 mm diameter pellets, and heated in air at 1200, 1300, 1350, and 1400 °C for 2 days at each temperature with intermediate grinding.

Fluorination of $Sr_3(M_{0.5}Ru_{0.5})_2O_7$ (M = Ti, Mn, Fe). Fluorination of $Sr_3(M_{0.5}Ru_{0.5})_2O_7$ (M = Ti, Mn, Fe) phases was carried out using CuF_2 as a solid-state fluorinating agent.[9] In order to investigate the reactivity of $Sr_3(M_{0.5}Ru_{0.5})_2O_7$ (M = Ti, Mn, Fe) phases with CuF_2, small-scale (~200 mg) test reactions were carried out by heating a variety of CuF_2:$Sr_3(M_{0.5}Ru_{0.5})_2O_7$ stoichiometric ratios under flowing oxygen at 250 °C. Samples suitable for neutron powder diffraction were prepared by grinding the $Sr_3(M_{0.5}Ru_{0.5})_2O_7$ (Fe, Mn) starting phases together with a double molar ratio of CuF_2 in an agate mortar and pestle and heating to 250 °C under flowing oxygen for three periods of 8 h to ensure that any excess CuF_2 was converted to CuO ($CuF_2 + 1/2O_2 \rightarrow CuO + F_2$).

Characterization. X-ray powder diffraction data were collected using a PANalytical X'Pert diffractometer in Bragg–Brentano geometry, incorporating an X'celerator position-sensitive detector (monochromatic Cu Kα_1 radiation). Neutron powder diffraction data were collected using the D2B diffractometer ($\lambda = 1.59$ Å) at the ILL neutron source (Grenoble, France) from samples contained within vanadium cans, sealed under argon with indium washers. Rietveld profile refinements were performed using the GSAS suite of programs.[20] Thermogravimetric data were collected using a Netzsch STA 409PC balance. Powder samples were heated under a flow of 25% H_2/75% N_2 at 10 °C min^{-1} to 800 °C and then held at this temperature for the remainder of the measurement. Magnetization measurements were collected using a Quantum Design MPMS SQUID magnetometer.

Room-temperature ^{57}Fe Mössbauer spectra were collected relative to α-Fe over the velocity range ±5 mm s^{-1} using a constant acceleration spectrometer with a 25 mCi source of ^{57}Co in Rh. The spectrum was satisfactorily fitted with two broadened Lorentzian paramagnetic doublets using the Recoil analysis software package.

The fluorine content of samples was determined spectrochemically using the lanthanum alizarin complexone method.[21,22] An alizarin complexone dye solution was prepared by combining 0.0599 g of alizarin complexone, 0.051 g of La_2O_3 (dissolved in a minimal amount of concentrated HCl), 10.25 g of sodium acetate, 7.5 mL of glacial acetic acid, and 125 mL of analytical reagent-grade acetone. The mixture was then made up to a volume of 250 mL with distilled water.[22] Small known quantities of fluorine-containing samples were dissolved in a minimal quantity of concentrated HCl. KOH was then added to precipitate the metal cations so they did not interfere with the measurement, and after filtration, the resulting solutions were made up to a known volume. The fluorine content of sample solutions was determined by adding known amounts of sample solution to 4 mL of dye solution, and then the mixture was then made up to a total volume of 25 mL with distilled water. The UV–vis spectrum of this solution was then recorded using a Perkin-Elmer Lambda 750S spectrometer in the range 1000–300 nm. The absorbance at 621 nm was measured, and the fluoride content was read from a calibration curve prepared from NaF solutions of known concentration.

RESULTS

Small-scale tests revealed that reactions between $Sr_3(M_{0.5}Ru_{0.5})_2O_7$ (M = Ti, Mn, Fe) phases and stoichiometric amounts of CuF_2 produced mixtures of $Sr_3(M_{0.5}Ru_{0.5})_2O_7$ starting material and a new phase. It was found that in order to form single-phase products an excess of CuF_2 was required. In addition, attempts were made to carry out the fluorination reaction while keeping the reactants segregated either by placing the $Sr_3(M_{0.5}Ru_{0.5})_2O_7$ phase and CuF_2 separately within the same reaction vessel or by placing pellet of the $Sr_3(M_{0.5}Ru_{0.5})_2O_7$ starting material on a bed of CuF_2. Both reaction set ups led to negligible amounts of the new products being produced, indicating that direct physical contact was necessary for formation of the desired phases. Thus, large-scale

dx.doi.org/10.1021/ic400125x | Inorg. Chem. 2013, 52, 3388–3398

samples were prepared using an intimately mixed 2:1 molar ratio of CuF_2:$Sr_3(M_{0.5}Ru_{0.5})_2O_7$.

Structural and Chemical Characterization of $Sr_3(Fe_{0.5}Ru_{0.5})_2O_xF_y$. X-ray powder diffraction data collected from the product of the reaction between $Sr_3(Fe_{0.5}Ru_{0.5})_2O_7$ and a double molar ratio of CuF_2 could be indexed on the basis of a tetragonal unit cell with space group *I*4/*mmm* and lattice parameters a = 3.89(1) Å and c = 23.53(1) Å. However, analogous neutron powder diffraction data exhibited additional diffraction peaks consistent with an $a' \approx \sqrt{2} \times a$, $b' \approx \sqrt{2} \times b$, $c' = c$ unit cell expansion of the majority phase. An analogous cell expansion has been observed in the fluorinated phase $Sr_3Ru_2O_7F_2$; therefore, a structural model based on the reported structure of $Sr_3Ru_2O_7F_2$ (space group *Pban*) was constructed and refined against the neutron diffraction data collected from $Sr_3(Fe_{0.5}Ru_{0.5})_2O_xF_y$ at 298 K. Since the neutron scattering lengths of oxide and fluoride are very similar (5.803 and 5.654 fm, respectively),[23] no attempt was made to distinguish between these anions in the structural model.

The cell expansion observed in the $Sr_3Ru_2O_7F_2$ structural model is attributable to the disordered twisting of RuO_6 octahedra, compared to the model in the unexpanded cell. This disordered twisting is described via partial occupation of pairs of symmetry-related equatorial anion sites. On refinement of the site occupancies of these equatorial anion sites, one site refined to full occupancy and the other to zero occupancy, indicating that in contrast to $Sr_3Ru_2O_7F_2$, $Sr_3(Fe_{0.5}Ru_{0.5})_2O_xF_y$ has an ordered twisting of $(Fe/Ru)O_xF_y$ octahedra. This observation allowed construction of a higher symmetry structural model in space group *Acaa* (No. 68), which gave a better statistical fit to the neutron diffraction data than the *Pban* model. Considering the chemical reaction used to prepare $Sr_3(Ru_{0.5}Fe_{0.5})_2O_xF_y$, CuO and CuF_2 were added to the refinement model as secondary phases; however, the phase fraction of CuF_2 rapidly refined to zero and was therefore eliminated from the refinement. The phase fraction of CuO rapidly refined to give a 2:1 molar ratio of CuO:$Sr_3(Fe_{0.5}Ru_{0.5})_2O_xF_y$, indicating that all the CuF_2 added to the reaction mixture had been converted to CuO. Refinement converged readily to give a good statistical fit. No significant deficiencies were observed in the occupations of any of the anion sites. Final refined structural parameters are listed in Table 1, and selected bond lengths and angles are listed in Table 2. Observed and calculated diffraction data are shown in Figure 2.

Thermogravimetric data collected during reduction of the $Sr_3(Fe_{0.5}Ru_{0.5})_2O_xF_y$ + CuO sample to SrO, SrF_2, Fe, Ru, and Cu (confirmed by X-ray diffraction) indicated a 13.6% mass loss (Supporting Information) consistent with the chemical composition $Sr_3(Fe_{0.5}Ru_{0.5})_2O_{5.46(5)}F_{3.54(5)}$. Spectrochemical fluorine analysis data collected from the fluorinated sample were also consistent with this formulation.

^{57}Fe Mössbauer spectra collected from $Sr_3(Fe_{0.5}Ru_{0.5})_2O_{5.5}F_{3.5}$ are shown in Figure 3 and can be fitted to two Lorentzian doublets as described in Table 3. The center shift and quadrupolar splitting parameters extracted from the fits to the data indicate that, within the sensitivity of the measurement, all iron in the sample is in the Fe^{3+} oxidation state and octahedrally coordinated. In addition, the data indicate that there are two iron sites in the sample which have similar quadrupolar splitting values, indicating similar levels of site distortion from perfect cubic symmetry, and that the sites are occupied in an approximate 2:1 ratio. These observations are consistent with 66% of the iron in $Sr_3(Fe_{0.5}Ru_{0.5})_2O_{5.5}F_{3.5}$ being located in $Fe^{3+}O_5F$ sites and 33% in $Fe^{3+}O_6$ sites, in line with the refined crystal structure of the phase.

Table 1. Parameters from Structural Refinement of $Sr_3(Fe_{0.5}Ru_{0.5})_2O_{5.5}F_{3.5}$ against Neutron Diffraction Data Collected at 298 K[a]

atom	x	y	z	U_{iso} (Å^2)
Sr(1)	3/4	1/4	0	0.009(1)
Sr(2)	3/4	1/4	0.1864(1)	0.007(1)
Ru/Fe	3/4	3/4	0.0828(1)	0.007(1)
X(1)	3/4	3/4	0	0.019(1)
X(2)	0.4670(9)	0.5329(9)	0.0842(1)	0.016(1)
X(3)	3/4	3/4	0.1645(2)	0.024(1)
X(4)	0.0002(16)	0	1/4	0.014(1)

[a] $Sr_3(Fe_{0.5}Ru_{0.5})_2O_{5.5}F_{3.5}$: Space group *Acaa*; a = 5.511(1) Å, b = 5.509(1) Å, c = 23.522(1) Å. Weight fraction: 77.8%. CuO: Space group *C*2/*c*; a = 4.676(1) Å, b = 3.430(1) Å, c = 5.129(1) Å, β = 98.97(2)°. Weight fraction: 22.2%. χ^2 = 7.220; wRp = 4.33%; Rp = 3.27%.

Table 2. Selected Bond Lengths (Angstroms) and Angles (degrees) for $Sr_3(Fe_{0.5}Ru_{0.5})_2O_{5.5}F_{3.5}$, $Sr_3(Mn_{0.5}Ru_{0.5})_2O_7F_2$, and $Sr_3(Ti_{0.5}Ru_{0.5})_2O_7F_2$ at Room Temperature

		$Sr_3(M_{0.5}Ru_{0.5})_2O_xF_y$		
		M = Fe	M = Mn	M = Ti
Sr(1)	X(1)	2 × 2.756(1)	2 × 2.700(1)	4 × 2.739(1)
	X(1)	2 × 2.755(1)	2 × 2.700(1)	
	X(2)	4 × 2.964(4)	4 × 2.948(5)	8 × 2.768(7)
	X(2)	4 × 2.605(5)	4 × 2.586(5)	
Sr(2)	X(2)	2 × 2.939(4)	2 × 2.942(5)	4 × 3.110(8)
	X(2)	2 × 3.262(4)	2 × 3.264(5)	
	X(3)	2 × 2.802(1)	2 × 2.747(1)	4 × 2.777(2)
	X(3)	2 × 2.803(1)	2 × 2.748(1)	
	X(4)	2 × 2.456(6)	2 × 2.460(3)	4 × 2.479(1)
	X(4)	2 × 2.457(5)	2 × 2.443(3)	
Ru/M	X(1)	1.948(2)	2.086(10)	2.075(2)
	X(2)	2 × 1.965(5)	2 × 1.928(5)	4 × 1.939(1)
	X(2)	2 × 1.966(6)	2 × 1.932(5)	
	X(3)	1.922(5)	1.838(11)	1.878(12)
Ru/M(1)−X(2)−Ru/M(1)		164.8(2)	161.5(2)	180
Ru/M(1)−X(1)−Ru/M(1)		179.9(2)	180.0(2)	180

Structural and Chemical Characterization of $Sr_3(Mn_{0.5}Ru_{0.5})_2O_xF_y$. X-ray powder diffraction data collected from the product of the reaction between $Sr_3(Mn_{0.5}Ru_{0.5})_2O_7$ and a double molar ratio of CuF_2 could be indexed on the basis of a tetragonal unit cell with space group *I*4/*mmm* and lattice parameters a = 3.81(1) Å and c = 23.89(1) Å. In common with $Sr_3(Fe_{0.5}Ru_{0.5})_2O_{5.5}F_{3.5}$, described above, neutron powder diffraction data collected from $Sr_3(Mn_{0.5}Ru_{0.5})_2O_xF_y$ exhibited additional diffraction peaks consistent with an $a' \approx \sqrt{2} \times a$, $b' \approx \sqrt{2} \times b$, $c' = c$ unit cell expansion of the majority phase. Therefore, the same refinement procedure described above for the Fe/Ru phase was followed for $Sr_3(Mn_{0.5}Ru_{0.5})_2O_xF_y$ using an analogous expanded structural model in space group *Acaa*. Again, CuO and CuF_2 were added to the structural model as secondary phases, with the fraction of CuF_2 rapidly refining to zero and the fraction of CuO rapidly refining to give a 2:1 molar ratio of CuO:$Sr_3(Mn_{0.5}Ru_{0.5})_2O_xF_y$. Refinement con-

dx.doi.org/10.1021/ic400125x | Inorg. Chem. 2013, 52, 3388−3398

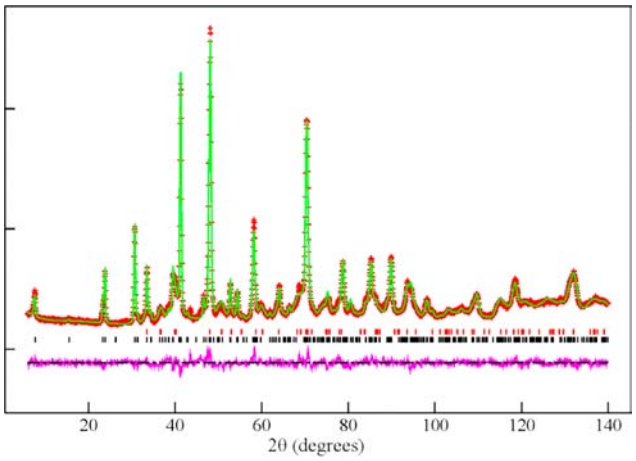

Figure 2. Observed calculated and difference plots from structural refinement of $Sr_3(Fe_{0.5}Ru_{0.5})_2O_{5.5}F_{3.5}$ against neutron powder diffraction data collected at room temperature. Tick marks indicate peak positions of the majority phase (bottom) and CuO secondary phase (top).

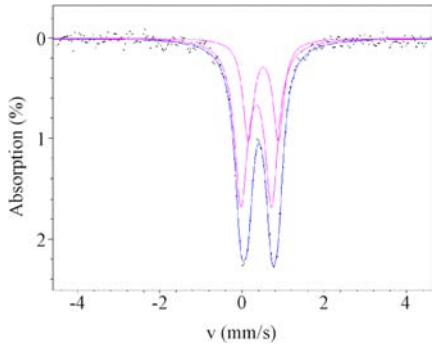

Figure 3. Fitted ^{57}Fe Mössbauer spectrum collected from $Sr_3(Ru_{0.5}Fe_{0.5})O_{5.5}F_{3.5}$ at room temperature.

Table 3. Parameters Extracted from Fitting Fe Mössbauer Spectra[a]

	site 1	site 2
center shift/mm s^{-1}	0.347	0.517
quadrupole splitting/mm s^{-1}	0.744	0.733
line width/mm s^{-1}	0.192	0.154
area fraction/%	66.6%	33.4%

[a]Center shift and quadrupole splitting parameters indicate that both sites correspond to octahedral Fe^{3+} centers.

verged readily to give a good statistical fit, and no significant deficiencies were observed in the occupancies of any anion sites. Final refined structural parameters are listed in Table 4, and selected bond lengths and angles are listed in Table 2. Observed and calculated diffraction data are shown in Figure 4.

Thermogravimetric data collected during reduction of the $Sr_3(Mn_{0.5}Ru_{0.5})_2O_xF_y$ + CuO sample to SrO, SrF_2, MnO, Ru, and Cu (confirmed by X-ray diffraction) indicated a 13.2% mass loss (Supporting Information) consistent with the chemical composition $Sr_3(Mn_{0.5}Ru_{0.5})_2O_{7.01(5)}F_{1.99(5)}$. Spectrochemical fluorine analysis data collected from the fluorinated sample were also consistent with this formulation.

Structural and Chemical Characterization of $Sr_3(Ti_{0.5}Ru_{0.5})_2O_7$ and $Sr_3(Ti_{0.5}Ru_{0.5})_2O_xF_y$. X-ray powder diffraction data collected from $Sr_3(Ti_{0.5}Ru_{0.5})_2O_7$, prepared as

Table 4. Parameters from Structural Refinement of $Sr_3(Mn_{0.5}Ru_{0.5})_2O_7F_2$ against Neutron Diffraction Data Collected at 298 K[a]

atom	x	y	z	U_{iso} (Å^2)
Sr(1)	3/4	1/4	0	0.012(1)
Sr(2)	3/4	1/4	0.1856(1)	0.003(1)
Ru/Mn	3/4	3/4	0.0874(4)	0.007(1)
X(1)	3/4	3/4	0	0.012(1)
X(2)	0.4655(9)	0.5341(8)	0.0835(2)	0.014(1)
X(3)	3/4	3/4	0.1644(2)	0.007(1)
X(4)	0.0037(14)	0	1/4	0.014(1)

[a]$Sr_3(Mn_{0.5}Ru_{0.5})_2O_7F_2$: Space group *Acaa*; a = 5.4028(9) Å, b = 5.4007(9) Å, c = 23.867(1) Å. Weight fraction: 77.6%. CuO: Space group *C2/c*; a = 4.676(1) Å, b = 3.430(1) Å, c = 5.129(1) Å, β = 98.97(2)°. Weight fraction: 22.4%. χ^2 = 7.260; wRp = 4.33%; Rp = 3.25%.

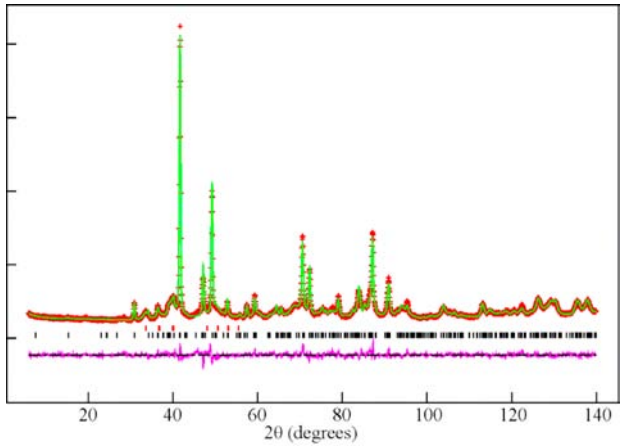

Figure 4. Observed, calculated, and difference plots from structural refinement of $Sr_3(Mn_{0.5}Ru_{0.5})_2O_7F_2$ against neutron powder diffraction data collected at room temperature. Tick marks indicate peak positions of the majority phase (bottom) and CuO secondary phase (top).

described above, could be readily indexed using a body-centered tetragonal unit cell with lattice parameters a = 3.9079(1) Å, c = 20.3792(1) Å, consistent with formation of a B-cation disordered n = 2 Ruddlesden–Popper phase. A structural model based on the reported structure of $Sr_3(Mn_{0.5}Ru_{0.5})_2O_7$,[19] but with manganese replaced by titanium, was refined against the X-ray diffraction data to a achieve a good statistical fit (χ^2 = 2.64). Full details of the refined structure of $Sr_3(Ti_{0.5}Ru_{0.5})_2O_7$ and a plot of the observed and calculated data are given in the Supporting Information.

X-ray powder diffraction data collected from the products of reaction between $Sr_3(Ti_{0.5}Ru_{0.5})_2O_7$ and a double molar ratio of CuF_2 could also be indexed using a body-centered tetragonal unit cell a = 3.8740(1) Å, c = 23.827(1) Å, consistent with topochemical fluorine insertion into the Ti/Ru phase. Therefore, a body-centered tetragonal structural model based on that refined for $Sr_3(Ti_{0.5}Ru_{0.5})_2O_7$, but with additional fluoride/oxide ions inserted into the SrO rock salt layers at (1/2, 0, 1/4), was refined against these data. Again, CuO and CuF_2 were added to the structural model as secondary phases, with the fraction of CuF_2 rapidly refining to zero and the fraction of CuO rapidly refining to give a 2:1 molar ratio of CuO:$Sr_3(Ti_{0.5}Ru_{0.5})_2O_xF_y$. Refinement converged rapidly to give a good statistical fit. An orthorhombic structural model in

dx.doi.org/10.1021/ic400125x | Inorg. Chem. 2013, 52, 3388–3398

space group *Acaa*, analogous to that used to describe $Sr_3(Mn_{0.5}Ru_{0.5})_2O_7$, was observed to give a worse statistical fit to the X-ray diffraction data than the *I*4/*mmm* model (*Acaa*: $\chi^2 = 2.98$; *I*4/*mmm*: $\chi^2 = 2.62$), and so the tetragonal model was retained. Full details of the refined structure are given in Table 5, with observed and calculated data shown in Figure 5.

Table 5. Parameters from Structural Refinement of $Sr_3(Ti_{0.5}Ru_{0.5})_2O_7F_2$ against X-ray Powder Diffraction Data Collected at 298 K[a]

atom	*x*	*y*	*z*	U_{iso} (Å^2)
Sr(1)	0	0	1/2	0.049(1)
Sr(2)	0	0	0.3149(1)	0.037(1)
Ru/Ti	0	0	0.0871(1)	0.024(1)
X(1)	0	0	0	0.035(1)
X(2)	0	1/2	0.0830(4)	0.035(1)
X(3)	0	0	0.1659(5)	0.035(1)
X(4)	0	1/2	1/4	0.035(1)

[a] $Sr_3(Ti_{0.5}Ru_{0.5})_2O_7F_2$: Space group *I*4/*mmm*; $a = 3.8740(1)$ Å, $c = 23.827(1)$ Å. Weight fraction: 82.1% . CuO: Space group *C*2/*c*; $a = 4.673(1)$ Å, $b = 3.432(1)$ Å, $c = 5.131(1)$ Å, $\beta = 98.98(2)°$. Weight fraction: 17.9% . $\chi^2 = 3.542$; wRp = 4.36%; Rp = 3.31%.

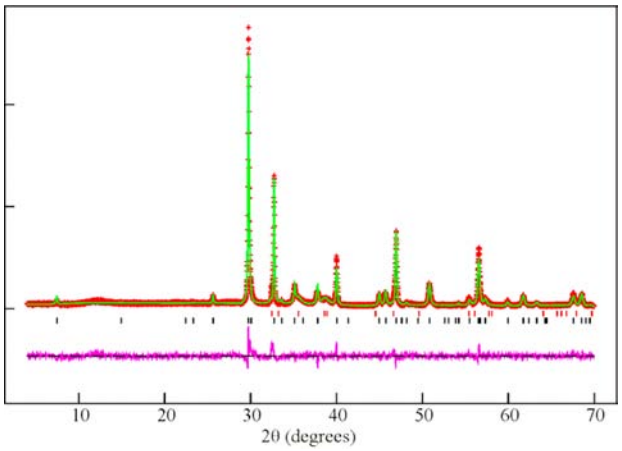

Figure 5. Observed, calculated, and difference plots from structural refinement of $Sr_3(Ti_{0.5}Ru_{0.5})_2O_7F_2$ against X-ray powder diffraction data collected at room temperature. Tick marks indicate peak positions of the majority phase (bottom) and the CuO secondary phase (top).

Thermogravimetric data collected during reduction of the $Sr_3(Ti_{0.5}Ru_{0.5})_2O_xF_y$ + CuO sample to SrO, SrF_2, TiO_2, Ru, and Cu (confirmed by X-ray diffraction) indicated a 11.1% mass loss (Supporting Information) consistent with the chemical composition $Sr_3(Ti_{0.5}Ru_{0.5})_2O_{6.97(5)}F_{2.03(5)}$. Spectrochemical fluorine analysis was not possible on this sample due to poor sample solubility.

Magnetic Characterization of $Sr_3(Fe_{0.5}Ru_{0.5})_2O_{5.5}F_{3.5}$. Magnetization data collected as a function of temperature from $Sr_3(Fe_{0.5}Ru_{0.5})_2O_{5.5}F_{3.5}$ are shown in Figure 6. Data in the range $140 \leq T/K \leq 300$ could be fitted to the Curie–Weiss law ($\chi = C/(T - \theta) + K$) to yield values of $C = 0.248(5)$ cm^3 K mol^{-1}, $\theta = 48.9(16)$ K, and $K = 0.0026(1)$ cm^3 mol^{-1}; however, it should be noted that due to the presence of CuO in the sample these values are hard to interpret. There is a divergence between the field-cooled and zero-field-cooled data sets at $T \approx 125$ K. Magnetization-field data collected at 300 K are linear and pass through the origin. In contrast, analogous data

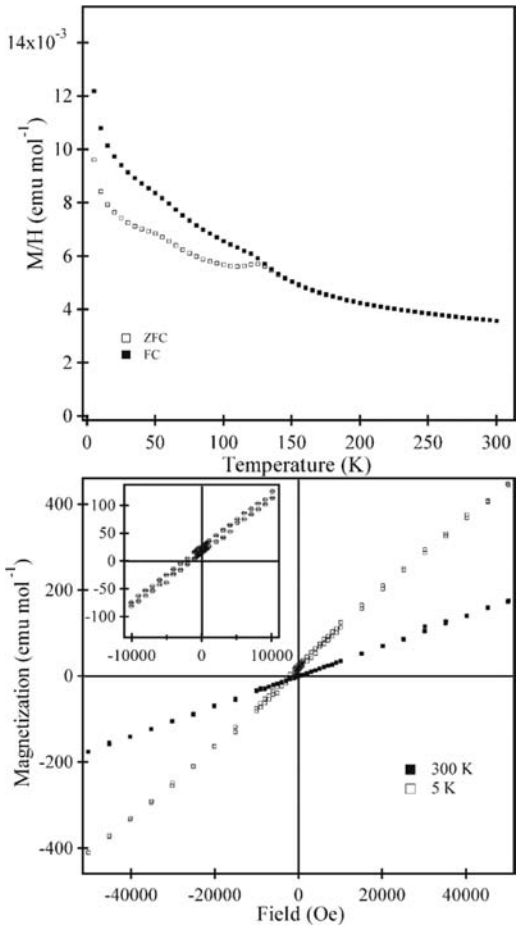

Figure 6. Zero-field-cooled and field-cooled magnetization data (top) and magnetization-field isotherms collected at 300 and 5 K (bottom) from $Sr_3(Fe_{0.5}Ru_{0.5})_2O_{5.5}F_{3.5}$.

collected at 5 K (Figure 6) exhibit hysteresis and are displaced from the origin, indicating a glassy component to the magnetic behavior.

Neutron powder diffraction data collected from $Sr_3(Fe_{0.5}Ru_{0.5})_2O_{5.5}F_{3.5}$ at 5 K exhibited additional features relative to the analogous data collected at 298 K. These additional diffraction features could be attributed to the presence of long-range magnetic order and indexed using a magnetic unit cell with the same dimensions as the crystallographic unit cell. Intensities of the magnetic scattering peaks could be best accounted from using a G-type antiferromagnetically ordered model, with spins aligned parallel to the crystallographic *c* axis (Figure 7). Refinement converged readily to yield an ordered moment of 1.12(3) μ_B per transition metal center. Complete details of the magnetic refinement are given in the Supporting Information.

Magnetic Characterization of $Sr_3(Ru_{0.5}Mn_{0.5})_2O_7F_2$. Magnetization data collected as a function of temperature from $Sr_3(Mn_{0.5}Ru_{0.5})_2O_7F_2$ (Figure 8) exhibit a local maximum at $T \approx 190$ K accompanied by a divergence between zero-field-cooled and field-cooled data. Data cannot be fitted to the Curie–Weiss law over any significant temperature range. Magnetization-field data collected at 300 K are linear and pass through the origin; however, analogous data collected at 5 K exhibit hysteresis and were displaced from the origin, consistent with glassy magnetic behavior. Neutron powder diffraction data collected from $Sr_3(Mn_{0.5}Ru_{0.5})_2O_7F_2$ at 5 K

dx.doi.org/10.1021/ic400125x | *Inorg. Chem.* 2013, 52, 3388–3398

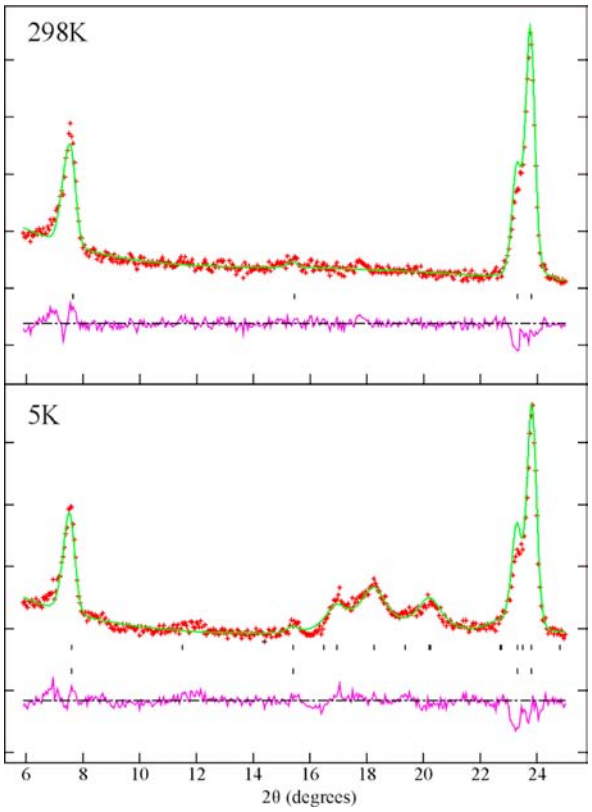

Figure 7. Observed, calculated, and difference plots from refinement of structural and magnetic models against neutron powder diffraction data collected from $Sr_3(Fe_{0.5}Ru_{0.5})_2O_{5.5}F_{3.5}$ at 298 and 5 K. Tick marks indicate peak positions for the structural (bottom) and magnetic (top) models.

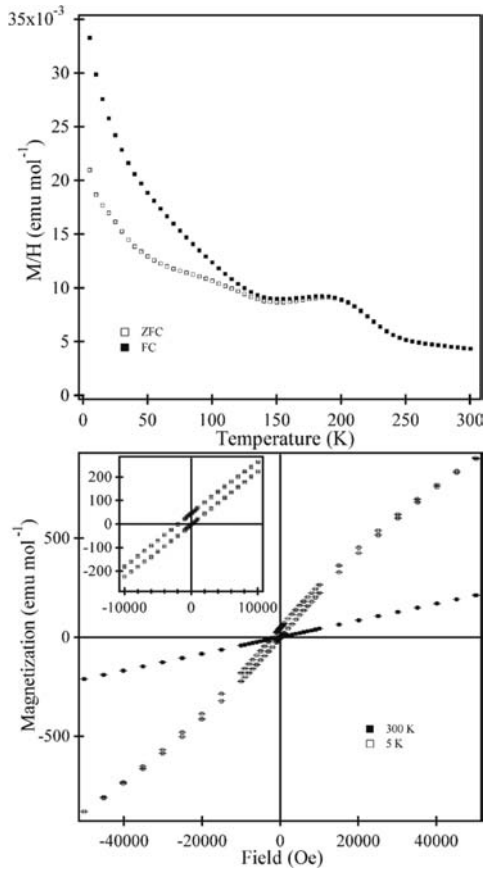

Figure 8. Zero-field-cooled and field-cooled magnetization data (top) and magnetization-field isotherms collected at 300 and 5 K (bottom) from $Sr_3(Mn_{0.5}Ru_{0.5})_2O_7F_2$.

exhibit weak, broad diffraction features compared to analogous data collected at 298 K (Figure 9). These additional diffraction features could be indexed using the crystallographic unit cell, but due to their weak intensities the data could not discriminate between a number of simple magnetic models; thus, no magnetic structural refinement is reported here.

Magnetic Characterization of $Sr_3(Ti_{0.5}Ru_{0.5})_2O_7$ and $Sr_3(Ti_{0.5}Ru_{0.5})_2O_7F_2$. Magnetization data collected as a function of temperature of $Sr_3(Ti_{0.5}Ru_{0.5})_2O_7$ are shown in Figure 10. Data in the range $80 \leq T/K \leq 300$ could be fitted to the Curie–Weiss law ($\chi = C/(T - \theta) + K$) to yield values of C = 1.622(5) cm^3 K mol^{-1}, $\theta = -27.4(3)$ K, and $K = 8 \times 10^{-5}$ cm^3 mol^{-1}. Below 80 K the zero-field- and field-cooled data diverge, indicative of a magnetic transition. Magnetization data collected as a function of temperature from $Sr_3(Ti_{0.5}Ru_{0.5})_2O_7F_2$ are shown in Figure 10. These data also exhibit a weak divergence between zero-field-cooled and field-cooled data at 80 K, which we ascribed to a very small amount of unfluorinated $Sr_3(Ti_{0.5}Ru_{0.5})_2O_7$ in the sample. Despite the presence of $Sr_3(Ti_{0.5}Ru_{0.5})_2O_7$ and CuO, data collected from the $Sr_3(Ti_{0.5}Ru_{0.5})_2O_7F_2$ sample could be fitted to the Curie–Weiss law over the temperature range $10 < T/K < 300$ to yield values C = 0.232(2) cm^3 K mol^{-1}, $\theta = -12.1(2)$ K, and $K = 2.32 \times 10^{-3}$ cm^3 mol^{-1}. Given the presence of 2 mol equiv of CuO in the sample, these should be considered as maximal values.

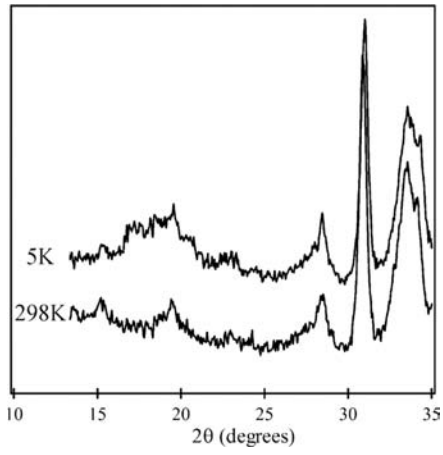

Figure 9. Neutron powder diffraction data collected from $Sr_3(Mn_{0.5}Ru_{0.5})_2O_7F_2$ at 298 and 5 K.

DISCUSSION

Reaction of $Sr_3(M_{0.5}Ru_{0.5})_2O_7$ (M = Ti, Mn, Fe) with CuF_2 under flowing oxygen leads to formation of $Sr_3(M_{0.5}Ru_{0.5})_2O_xF_y$ oxide–fluoride phases via a topochemical fluorination process. In the case of $Sr_3(Mn_{0.5}Ru_{0.5})_2O_7$ and $Sr_3(Ti_{0.5}Ru_{0.5})_2O_7$ this process is a simple oxidative insertion, leading to formation of $Sr_3(Mn_{0.5}Ru_{0.5})_2O_7F_2$ and $Sr_3(Ti_{0.5}Ru_{0.5})_2O_7F_2$, respectively, and a change in the average transition metal oxidation state from M^{4+} to M^{5+}. In contrast, reaction with $Sr_3(Fe_{0.5}Ru_{0.5})_2O_7$ has a significant substitutive component, both inserting fluoride

dx.doi.org/10.1021/ic400125x | Inorg. Chem. 2013, 52, 3388–3398

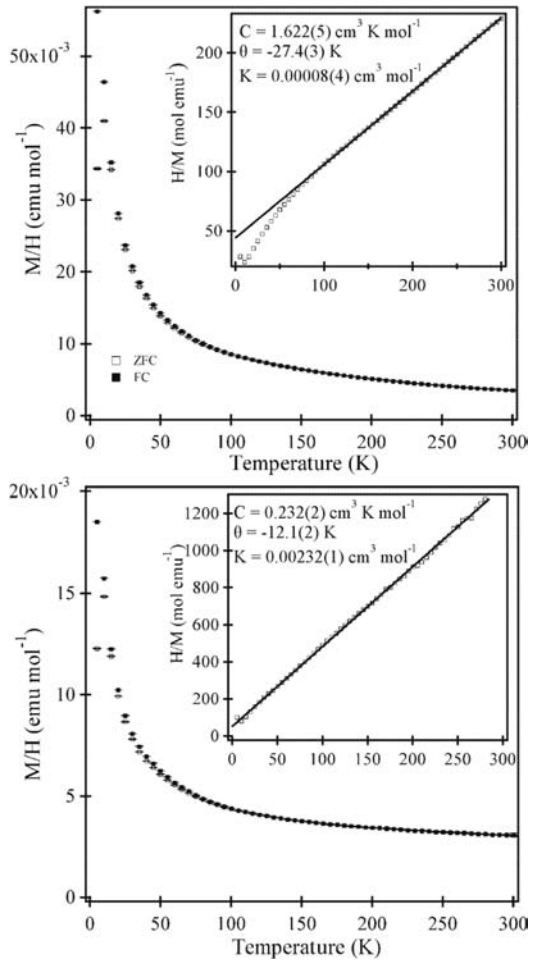

Figure 10. Magnetization data collected from $Sr_3(Ti_{0.5}Ru_{0.5})_2O_7$ (top) and $Sr_3(Ti_{0.5}Ru_{0.5})_2O_7F_2$ (bottom) as a function of temperature. (Insets) Fits to the Curie–Weiss law: $\chi = C/(T - \theta) + K$.

ions into the host structure and exchanging some of the existing framework oxide ions for fluoride ions, to form $Sr_3(Mn_{0.5}Ru_{0.5})_2O_{5.5}F_{3.5}$. As a result, the average transition metal oxidation state in this case changes only modestly from M^{4+} to $M^{4.25+}$.

Distribution of Oxide and Fluoride Ions. Crystal structures of the $Sr_3(M_{0.5}Ru_{0.5})_2O_xF_y$ oxide–fluoride phases contain an additional anion site, compared to the $Sr_3(M_{0.5}Ru_{0.5})_2O_7$ starting materials, located within the SrX rock salt layers of the lattice, which allows the higher anion stoichiometry of these phases to be accommodated (Figure 1). As a result, the oxide–fluoride phases have four crystallographically distinct anion sites within their crystal structures, as shown in Figure 1. As noted previously, the neutron and X-ray scattering lengths of O^{2-} and F^- are so similar as to provide no scattering contrast between the two different anions,[23] preventing direct determination of the distribution of oxide and fluoride ions within oxide–fluoride phases by either diffraction technique. However, it is possible to deduce the oxide/fluoride distributions in some oxide–fluoride phases by detailed examination of the local bonding at anion sites, via bond valence sums (BVS).[21,24] Table 6 lists the bond valence sums calculated for the oxide ion sites of $Sr_3(Mn_{0.5}Ru_{0.5})_2O_7$ and the anion sites of the $Sr_3(Mn_{0.5}Ru_{0.5})_2O_7F_2$ calculated as if the sites were occupied by either oxide or fluoride ions. Examination of these values reveals that the interstitial anion

Table 6. Bond Valence Sums (BVS) Calculated for Anion Sites in $Sr_3(M_{0.5}Ru_{0.5})_2O_7$ and $Sr_3(M_{0.5}Ru_{0.5})_2O_xF_y$ (M = Mn, Fe, Ti) Phases, with Values for the Latter Phase Calculated for Occupation by Both Oxide and Fluoride Ions[a]

$Sr_3(Mn_{0.5}Ru_{0.5})_2O_7$		$Sr_3(Mn_{0.5}Ru_{0.5})_2O_7F_2$		
anion	BVS (O)	anion	BVS (O)	BVS (F)
O(1)	2.205	X(1)	**1.841**	1.419
O(2)	2.320	X(2)	**2.040**	1.578
O(3)	1.785	X(3)	**1.719**	1.320
		X(4)	1.647	**1.260**
$Sr_3(Fe_{0.5}Ru_{0.5})_2O_7$		$Sr_3(Fe_{0.5}Ru_{0.5})_2O_{5.5}F_{3.5}$		
anion	BVS (O)	anion	BVS (O)	BVS (F)
O(1)	1.911	X(1)	**2.184**	1.687
O(2)	2.225	X(2)	**1.924**	1.487
O(3)	1.751	X(3)	1.417	**1.092**
		X(4)	1.602	**1.226**
$Sr_3(Ti_{0.5}Ru_{0.5})_2O_7$		$Sr_3(Ti_{0.5}Ru_{0.5})_2O_7F_2$		
anion	BVS (O)	anion	BVS (O)	BVS (F)
O(1)	1.855	X(1)	**1.789**	1.380
O(2)	1.996	X(2)	**2.196**	1.696
O(3)	1.764	X(3)	**1.538**	1.220
		X(4)	1.507	**1.153**

[a]All values calculated using the Ru^{4+} parameter for contributions from all mixed M/Ru cation sites.

site (X(4)) has the lowest bond valence sum of all the anion sites in $Sr_3(Mn_{0.5}Ru_{0.5})_2O_7F_2$, consistent with the location of fluoride ions within this site. This is reinforced by the observation that the Sr(2)–X(4) bond length (2.45 Å) is very similar to the Sr–F bond length observed in SrF_2 (2.511 Å)[25] and those observed in $Sr_3Ru_2O_7F_2$ (2.32–2.56 Å).[9] Thus, we can conclude that fluorination of $Sr_3(Mn_{0.5}Ru_{0.5})_2O_7$ proceeds via the simple, topochemical insertion of fluoride ions into the interstitial anion sites of the host phase (Figure 1) in a manner directly analogous to fluorination of $Sr_3Ru_2O_7$ to $Sr_3Ru_2O_7F_2$.[9] A similar situation can be observed in the bond valence sums calculated for $Sr_3(Ti_{0.5}Ru_{0.5})_2O_7F_2$ (Table 6), although in this instance the poor X-ray scattering power of the light oxide and fluoride ions compared to the heavier metal cations reduces the certainty with which the anion positions are known (particularly X(3)), making this result less clear.

Close examination of the structure of $Sr_3(Fe_{0.5}Ru_{0.5})_2O_{5.5}F_{3.5}$ reveals a different picture. Bond valence sums (Table 6) reveal that in common with $Sr_3(Mn_{0.5}Ru_{0.5})_2O_7F_2$ and $Sr_3(Ti_{0.5}Ru_{0.5})_2O_7F_2$, the BVS of the X(4) interstitial anion site is in the range expected if this site were occupied by fluoride ions rather than an oxide ions, with the Sr(2)–X(4) bond length (2.45 Å) again being similar to the Sr–F bond length in SrF_2 (2.511 Å).[25] However, it can also be seen in Table 6 that the BVS of the X(3) anion site has declined significantly on fluorination, from +1.751 in $Sr_3(Fe_{0.5}Ru_{0.5})_2O_7$ to +1.417 in $Sr_3(Fe_{0.5}Ru_{0.5})_2O_{5.5}F_{3.5}$ (values calculated using oxide ion BVS parameters), suggesting this site is occupied by significant concentration of fluoride ions in the fluorinated phase. Considering the chemical formula of $Sr_3(Fe_{0.5}Ru_{0.5})_2O_{5.5}F_{3.5}$, we therefore propose that the X(1) and X(2) anion sites of the oxide–fluoride phase are occupied by oxide ions, the X(4) site by fluoride ions, and the X(3) site by a 75%/25% F^-/O^{2-} combination (Figure 1). A similar tendency to locate fluoride ions within the external axial anion

dx.doi.org/10.1021/ic400125x | Inorg. Chem. 2013, 52, 3388–3398

sites of $n = 2$ Ruddlesden–Popper phases was observed by Weller et al. during fluorination of $Sr_3Fe_2O_6$ to $Sr_3Fe_2O_6F_{0.98}$.[21]

The proposed distribution of oxide and fluoride ions within the $Sr_3(Fe_{0.5}Ru_{0.5})_2O_{5.5}F_{3.5}$ lattice is also consistent with the ^{57}Fe Mössbauer data collected from this phase. These data indicate that there are two octahedral iron sites within the material which we assign as an FeO_6 coordination and an FeO_5F coordination in which the fluoride ion is located in the X(3) anion site. However, the observed 2:1 ratio of FeO_5F:FeO_6 is slightly less than the 3:1 ratio expected from a statistical distribution of a 75% occupancy of fluoride ions over all available X(3) sites, suggesting a preferential substitution of fluoride for oxide at X(3) sites coordinated to ruthenium cations rather than iron cations to give a RuO_5F:RuO_6 ratio of 5:1.

Transition Metal Oxidation States. Magnetization data collected from $Sr_3(Ti_{0.5}Ru_{0.5})_2O_7$ are consistent with a transition metal oxidation state combination of Ti^{4+}/Ru^{4+} (Figure 10). Oxidative insertion of fluorine into $Sr_3(Ti_{0.5}Ru_{0.5})_2O_7$ to form $Sr_3(Ti_{0.5}Ru_{0.5})_2O_7F_2$ raises the average transition metal oxidation state from M^{4+} in the oxide to M^{5+} in the oxide–fluoride phase. Given the extreme thermodynamic unfavorability of oxidizing Ti^{4+}, this implies a transition metal oxidation state combination of $Sr_3(Ti^{4+}_{0.5}Ru^{6+}_{0.5})_2O_7F_2$; thus, it can be seen that Ru^{4+} is oxidized to Ru^{6+} under the applied 'soft' fluorination conditions.

Previous structural and magnetic studies by Battle et al. have shown that the transition metal oxidation state combination in $Sr_3(Fe_{0.5}Ru_{0.5})_2O_7$ is Fe^{3+}/Ru^{5+}.[18] As noted above, fluorination of $Sr_3(Fe_{0.5}Ru_{0.5})_2O_7$ with CuF_2/O_2 has a large substitutive component, so the fluorinated product phase has a composition of $Sr_3(Fe_{0.5}Ru_{0.5})_2O_{5.5}F_{3.5}$, yielding an average transition metal oxidation state of $M^{4.25+}$. ^{57}Fe Mössbauer spectra collected from $Sr_3(Fe_{0.5}Ru_{0.5})_2O_{5.5}F_{3.5}$ indicate an iron oxidation state of Fe^{3+}, which means the transition metal oxidation state combination in the fluorinated phase is $Sr_3(Fe^{3+}_{0.5}Ru^{5.5+}_{0.5})_2O_{5.5}F_{3.5}$, so again Ru^{6+} centers have been formed under the soft fluorination conditions applied. The large substitutive component of the fluorination reaction of $Sr_3(Fe_{0.5}Ru_{0.5})_2O_7$ compared to $Sr_3(Ti_{0.5}Ru_{0.5})_2O_7$ indicates that the Fe/Ru metal combination is less readily oxidized than the Ti/Ru combination. While this difference can be principally attributed to the thermodynamic difficulty of oxidizing Fe^{3+} to Fe^{4+} under the applied reaction conditions, formation of an $Fe^{3+}/Ru^{5.5+}$ phase ($Sr_3(Fe_{0.5}Ru_{0.5})_2O_{5.5}F_{3.5}$) rather than an Fe^{3+}/Ru^{6+} phase (analogous to the Ti^{4+}/Ru^{6+} phase $Sr_3(Ti_{0.5}Ru_{0.5})_2O_7F_2$) indicates more subtle factors are restricting the degree of oxidation of ruthenium during the fluorination reaction.

The transition metal oxidation state combination present in $Sr_3(Mn_{0.5}Ru_{0.5})_2O_7F_2$ is less clear. Previous studies have demonstrated an Mn^{4+}/Ru^{4+} combination for $Sr_3(Mn_{0.5}Ru_{0.5})_2O_7$.[19] Oxidative insertion of fluorine to form $Sr_3(Mn_{0.5}Ru_{0.5})_2O_7F_2$ raises the average transition metal oxidation state to M^{5+}, consistent with either Mn^{4+}/Ru^{6+} or Mn^{5+}/Ru^{5+}. In the absence of a direct measure of either the manganese or ruthenium oxidation states this issue will remain ambiguous; however, it should be noted that the attempted fluorination of $Ca_3Mn_2O_7$ with CuF_2/O_2 was unsuccessful, suggesting oxidation of Mn^{4+} is not possible under these soft conditions, supporting a Mn^{4+}/Ru^{6+} combination. As noted previously, the presence of CuO in the sample prevents an oxidation state assignment on the basis of magnetic behavior.

As described above, under the soft fluorination conditions utilized in this study CuF_2 acts as a fluorine source not an oxidant. The oxidizing 'power' of the reaction is instead supplied by the oxygen atmosphere as shown in reaction 1.

$$Sr_3(Ti_{0.5}Ru_{0.5})_2O_7 + CuF_2 + 0.5O_2 \rightarrow Sr_3(Ti_{0.5}Ru_{0.5})_2O_7F_2 + CuO \quad (1)$$

It is therefore a little surprising to prepare phases containing Ru^{6+} centers under these conditions, as stabilization of such a high ruthenium oxidation state typically requires high oxygen pressures. For example, formation of stoichiometric $Tl_2Ru_2O_7$ requires 1 GPa of oxygen pressure, while preparation of $Sr_2Ru_3O_{10}$ requires ~0.2 GPa pressure.[26,27] There are however examples of Ru^{6+} oxides prepared under ambient pressure conditions, particularly when group 1 (Na, K, Rb) peroxides or superoxides are employed as reagents. Thus, for example, A_2RuO_4 (A = Na, K, Rb) phases can be prepared by heating A_2O_2 with RuO_2 under flowing oxygen at modest temperature ($T < 720$ °C).[28,29] These reactions are strongly reminiscent of the use of metal hydroxide fluxes as strongly oxidizing media to stabilize high transition metal oxidation states.[30] Under the reaction conditions employed, metal hydroxide fluxes react with oxygen to form peroxide and superoxide anion in situ. These anions, in combination with the low synthesis temperatures employed, favor highly oxidized products. A similar explanation can be applied to rationalize the oxidizing power of the CuF_2/O_2 system: the high lattice energy gain associated with inserting small fluoride anions in combination with low synthesis temperatures favor anion-rich oxidized phases, thus enabling formation of highly oxidized products.

Magnetic Behavior. As noted above, the topochemical fluorination of $Sr_3(M_{0.5}Ru_{0.5})_2O_7$ (M = Ti, Mn, Fe) phases raises the oxidation state of the ruthenium centers in the $Sr_3(M_{0.5}Ru_{0.5})_2O_xF_y$ products while leaving the oxidation states of the other transition metal M cations unchanged. Despite this common chemical feature, fluorination reactions have a strikingly different effect on the magnetic behavior of the different materials studied.

$Sr_3(Ti_{0.5}Ru_{0.5})_2O_7$ exhibits Curie–Weiss paramagnetism above 80 K, below which temperature it is assumed to adopt an antiferromagnetically ordered state. It should be noted that the observed Curie constant of $Sr_3(Ti_{0.5}Ru_{0.5})_2O_7$ is significantly larger than that predicted by the spin-only formula as shown in Figure 10 ($C_{expected}$ = 1 cm^3 K mol^{-1}, $C_{observed}$ = 1.622(5) cm^3 K mol^{-1}). Fluorination of $Sr_3(Ti_{0.5}Ru_{0.5})_3O_7$ to form $Sr_3(Ti_{0.5}Ru_{0.5})_3O_7F_2$ leads to a suppression of the magnetic ordering transition, a dramatic drop in the observed Curie constant, and a significant rise in the temperature-independent paramagnetic (TIP) contribution to the magnetic response of the oxide–fluoride phase, compared to the all oxide parent material. In contrast, $Sr_3(Fe_{0.5}Ru_{0.5})_2O_7$ and $Sr_3(Mn_{0.5}Ru_{0.5})_2O_7$ exhibit spin-glass behavior at low temperature. Fluorination to form $Sr_3(Fe_{0.5}Ru_{0.5})_2O_{5.5}F_{3.5}$ and $Sr_3(Mn_{0.5}Ru_{0.5})_2O_7F_2$ appears to relieve the magnetic frustration of the parent phases, allowing the oxide–fluoride materials to exhibit long-range magnetic order.

The contrasting magnetic behavior of the different $Sr_3(M_{0.5}Ru_{0.5})_2O_xF_y$ phases can be rationalized by considering previous analysis by Goodenough, which provides some guidance as to the changes in magnetic coupling strength expected on changing transition metal oxidation states.[2] Figure 11 shows a simplified schematic phase diagram of the transfer

dx.doi.org/10.1021/ic400125x | Inorg. Chem. 2013, 52, 3388–3398

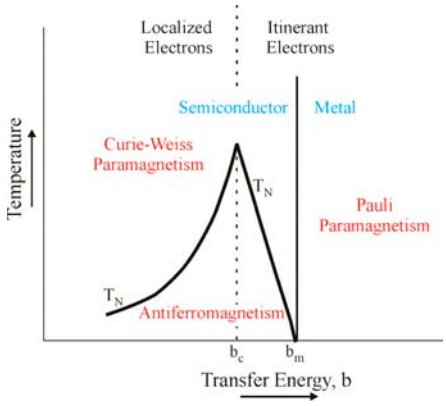

Figure 11. Simplified temperature-transfer integral phase diagram for one electron per orbital.

energy b, which is a measure of the strength of interaction between like atoms, against temperature. As shown in Figure 11, as the size of b increases from some small value, materials will change from localized electron insulators/semiconductors to itinerant electron metals at some critical value b_m. The change in the strength of magnetic superexchange coupling interactions as a function of b is more complex. As b increases from some small value, the strength of superexchange coupling between neighboring atoms increases, leading to a corresponding increase in the magnetic ordering temperature, T_N, as shown in Figure 11. However, at some critical value b_c, some of the electrons in the system become itinerant, screening the magnetic couplings between neighboring atoms, weakening the magnetic superexchange coupling, and leading to a decline in T_N with increasing b, until metallic Pauli paramagnetism is observed at b_m. In this intermediate $b_c < b < b_m$ range, interactions between localized and itinerant electrons lead to strong deviations from simple Curie–Weiss paramagnetic behavior, with observed Curie constants exceeding those calculated using the spin-only formula.[2]

Previous studies by Goodenough and Battle suggest that ruthenium oxides with ruthenium oxidation states in the $Ru^{4+/5+}$ range reside in this intermediate $b_c < b < b_m$ regime.[31] Thus, it is no surprise that $Sr_3(Ti_{0.5}Ru_{0.5})_2O_7$ exhibits an anomalously large Curie constant, as also observed for related Ru^{4+} double perovskites such as La_2MgRuO_6 and La_2ZnRuO_6.[32] Raising the oxidation state of a transition metal center will tend to increase the transfer energy of the system because oxidation lowers the energy of the metal orbitals, leading to a widening of the bands derived from the metal d orbitals (particularly the π^* bands) due to stronger metal d → oxygen 2p orbital interaction/hybridization. Thus, fluorination of $Sr_3(Ti_{0.5}Ru_{0.5})_2O_7$ to $Sr_3(Ti_{0.5}Ru_{0.5})_2O_7F_2$ would be expected to increase b, explaining the suppression of magnetic order, decline in Curie constant, and increase in TIP as the oxide–fluoride phase approaches itinerant metallic behavior. Thus, the magnetic behavior of the Ti/Ru phases can be readily explained by the ideas expressed in Figure 11.

Analysis of the Fe/Ru and Mn/Ru systems is more complex. Battle et al. pointed out that when considered simply, the magnetic superexchange couplings present in $Sr_3(Fe_{0.5}Ru_{0.5})_2O_7$ should not be frustrated.[18] The Goodenough–Kanamouri rules[33] indicate that the 180° σ-type magnetic superexchange couplings between nearest-neighbor Fe^{3+} $t_{2g}^3e_g^2$ and Ru^{5+} $t_{2g}^3e_g^0$ centers should be as follows: Fe–O–Fe, antiferromagnetic ($J^{nn}_{Fe/Fe} < 0$); Ru–O–Ru antiferromagnetic ($J^{nn}_{Ru/Ru} < 0$); Fe–O–Ru ferromagnetic ($J^{nn}_{Fe/Ru} > 0$). These pairwise magnetic couplings can be satisfied for all Fe/Ru arrangements. This can most easily been seen by first considering an all-iron system in which the $J^{nn}_{Fe/Fe}$ coupling leads to G-type antiferromagnetic order in which the spin on each iron center is antiparallel to those of all its nearest neighbors (Figure 12a). Random substitution of one-half the

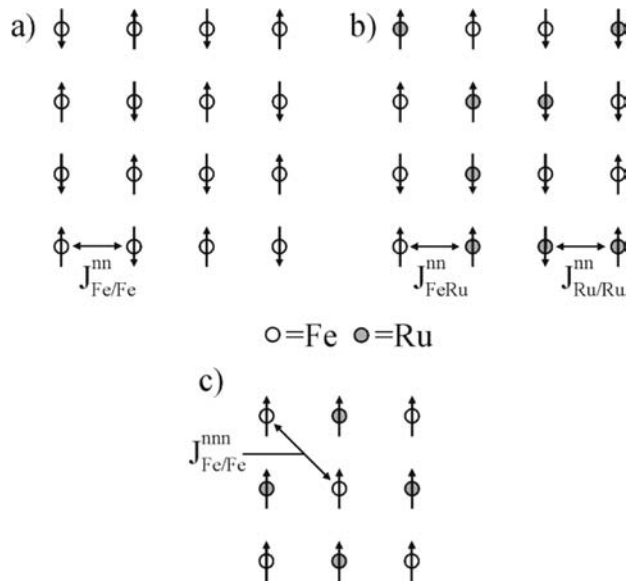

Figure 12. (a) G-type antiferromagnetically ordered structure of a square lattice of Fe^{3+}. (b) 'Antiferromagnetic' spin arrangement of a disordered array of Fe^{3+} and Ru^{5+}. (c) Strong antiferromagnetic $J^{nnn}_{Fe/Fe}$ couplings lead to frustration in some Fe^{3+}/Ru^{5+} arrangements.

iron centers with ruthenium to form the $Sr_3(Fe_{0.5}Ru_{0.5})_2O_7$ lattice can be achieved while satisfying the magnetic couplings described above by inverting the spin direction at each site where ruthenium is substituted, as shown in Figure 12b. Thus, by this simple analysis we would expect $Sr_3(Fe_{0.5}Ru_{0.5})_2O_7$ to adopt an antiferromagnetically ordered state with an average ordered moment at each transition metal site equal to the difference between the local iron and the ruthenium moments divided by two, i.e., $(5 - 3)/2 = 1\ \mu_B$. The fact that spin-glass behavior, not antiferromagnetism, is observed for $Sr_3(Fe_{0.5}Ru_{0.5})_2O_7$ indicates a more complex situation. Battle et al. suggested that the observed magnetic behavior arises from a mismatch between the strong exchange interactions of 3d iron centers compared to the relatively weak exchange interactions of 4d ruthenium centers.[18] As a result, $|J^{nn}_{Fe/Fe}| \gg |J^{nn}_{Fe/Ru}| \approx |J^{nn}_{Ru/Ru}| \approx |J^{nnn}_{Fe/Fe}|$, that is, the next-nearest-neighbor coupling between two iron centers is comparable to any nearest-neighbor interaction involving ruthenium. When these antiferromagnetic next-nearest-neighbor interactions are considered some arrangements of iron and ruthenium centers become magnetically frustrated, as shown in Figure 12c, explaining the observed magnetic behavior.

$Sr_3(Fe_{0.5}Ru_{0.5})_2O_{5.5}F_{3.5}$ adopts an antiferromagnetically ordered state below 125 K, indicating that fluorination of $Sr_3(Fe_{0.5}Ru_{0.5})_2O_7$ lifts the magnetic frustration of the Fe/Ru lattice. The only way that the frustration can be lifted, consistent with the observed magnetic behavior of $Sr_3(Fe_{0.5}Ru_{0.5})_2O_{5.5}F_{3.5}$, is if the ruthenium nearest-neighbor magnetic exchange interactions are strengthened relative to next-nearest-neighbor iron–iron exchange interactions, as the

dx.doi.org/10.1021/ic400125x | Inorg. Chem. 2013, 52, 3388–3398

σ-type superexchange couplings of Ru^{6+} are predicted to be of the same sign as Ru^{5+}. The result would be an antiferromagnetic ordered arrangement of iron and ruthenium spins as shown in Figure 12b, with an average ordered moment of 1.25 μ_B per transition metal center, consistent with the observed antiferromagnetic behavior of $Sr_3(Fe_{0.5}Ru_{0.5})_2O_{5.5}F_{3.5}$ (observed ordered moment =1.12(3) μ_B). Such a strengthening of the ruthenium superexchange interactions appears to contradict the increase in b and thus *decrease* in ruthenium superexchange strength expected on fluorination due to oxidation of Ru^{5+} to $Ru^{5.5+}$. However, the change in ruthenium oxidation state is not the only parameter which determines the change in transfer energy on fluorination. As noted above, fluorination of $Sr_3(Fe_{0.5}Ru_{0.5})_2O_7$ to $Sr_3(Fe_{0.5}Ru_{0.5})_2O_{5.5}F_{3.5}$ results in a lowering of crystallographic symmetry from tetragonal to orthorhombic, associated with a distortion in the (Fe/Ru)−O−(Fe/Ru) bond angle from 180° to 164.8(2)° (Table 2). This tightening of the (Fe/Ru)−O−(Fe/Ru) bond angle will lead to a narrowing of the bands derived from the ruthenium d orbitals, leading to a decrease in b and the observed strengthening on the ruthenium superexchange interactions. This picture is also consistent with the observation that the all-ruthenium phase $Sr_3Ru_2O_7F_2$ has both the highest magnetic ordering temperature ($T_N \approx 185$ K) and the tightest Ru−O−Ru bond angles (158.1°, 154.1°) of all ruthenium-containing oxide−fluoride phases studied, despite containing Ru^{5+} centers.[9]

The Mn/Ru phases appear to adopt the same behavior as the Fe/Ru phases. On fluorination the (Mn/Ru)−O−(Mn/Ru) bond angle contracts to 161.5° (Table 2), strengthening the ruthenium superexchange couplings and lifting the magnetic frustration in the fluorinated phase. A disordered arrangement of d^3 Mn^{4+} and d^2 Ru^{6+} would yield an antiferromagnetic state with an average ordered moment of (3−2)/2 = 0.5 μ_B per transition metal center, hence the weak magnetic diffraction peaks observed for this phase at low temperature (Figure 9).

Magnetization data collected from $Sr_3(Fe_{0.5}Ru_{0.5})_2O_{5.5}F_{3.5}$ and $Sr_3(Mn_{0.5}Ru_{0.5})_2O_7F_2$ (Figures 6 and 8) show there is still a small glassy component to the magnetic behavior of these phases, indicating that although the magnetic frustration has been lifted from the majority of the samples there remain some frustrated M/Ru configurations. This suggests that the strengthening of the ruthenium superexchange interactions on fluorination is not sufficient to completely remove the influence of the $J^{nnn}_{Fe/Fe}$ and $J^{nnn}_{Mn/Mn}$ couplings in the materials.

CONCLUSION

Reaction of $Sr_3(M_{0.5}Ru_{0.5})_2O_7$ (M = Ti, Mn, Fe), n = 2, Ruddlesden−Popper phases with CuF_2 under flowing oxygen leads to the topochemical insertion/exchange of fluoride ions and formation of $Sr_3(M_{0.5}Ru_{0.5})_2O_xF_y$ oxide−fluoride phases. Anion insertion/exchange reactions oxidize the host lattice and result in formation of Ru^{6+} centers under rather 'soft' conditions, allowing the complex magnetic couplings present in the parent materials to be tuned by a combination of electronic and structural interactions. It is reasonable to think that the reactions utilized in this study can be applied more widely, enabling further materials with exotic electronic configurations to be prepared and studied.

ASSOCIATED CONTENT

Supporting Information

Thermogravimetric data collected during reduction of $Sr_3(Fe_{0.5}Ru_{0.5})_2O_{5.5}F_{3.5}$, $Sr_3(Mn_{0.5}Ru_{0.5})_2O_7F_2$, and $Sr_3(Ti_{0.5}Ru_{0.5})_2O_7F_2$; structural parameters and observed and calculated diffraction data from refinement of $Sr_3(Ti_{0.5}Ru_{0.5})_2O_7$; parameters from structural and magnetic refinement of $Sr_3(Fe_{0.5}Ru_{0.5})_2O_{5.5}F_{3.5}$ against neutron diffraction data collected at 5 K. This material is available free of charge via the Internet at http://pubs.acs.org.

AUTHOR INFORMATION

Corresponding Author

*E-mail: michael.hayward@chem.ox.ac.uk.

Author Contributions

The manuscript was written through contributions of all authors.

Notes

The authors declare no competing financial interest.

ACKNOWLEDGMENTS

We thank E. Suard for assistance collecting the neutron powder diffraction data.

REFERENCES

(1) Goodenough, J. B.; Zhou, J.-S. *Chem. Mater.* **1998**, *10*, 2980.
(2) Goodenough, J. B. *Prog. Solid State Chem.* **1971**, 5.
(3) Hayward, M. A.; Green, M. A.; Rosseinsky, M. J.; Sloan, J. *J. Am. Chem. Soc.* **1999**, *121*, 8843.
(4) Seddon, J.; Suard, E.; Hayward, M. A. *J. Am. Chem. Soc.* **2010**, *132*, 2802.
(5) Dixon, E.; Hadermann, J.; Ramos, S.; Goodwin, A. L.; Hayward, M. A. *J. Am. Chem. Soc.* **2011**, *133*, 18397.
(6) Gopalakrishnan, J. *Chem. Mater.* **1995**, *7*, 1265.
(7) Schaak, R. E.; Mallouk, T. E. *Chem. Mater.* **2002**, *14*, 1455.
(8) Ranmohotti, K. G. S.; Josepha, E.; Choi, J.; Zhang, J. X.; Wiley, J. B. *Adv. Mater.* **2011**, *23*, 442.
(9) Li, R. K.; Greaves, C. *Phys. Rev. B* **2000**, *62*, 3811.
(10) Girgsdies, F.; Schollhorn, R. *Solid State Commun.* **1994**, *91*, 111.
(11) Jorgensen, J. D.; Dabrowski, B.; Pei, S.; Richards, D. R.; Hinks, D. G. *Phys. Rev. B* **1989**, *40*, 2187.
(12) Jorgensen, J. D.; Dabrowski, B.; Pei, S. Y.; Hinks, D. G.; Soderholm, L.; Morosin, B.; Schirber, J. E.; Venturini, E. L.; Ginley, D. S. *Phys. Rev. B* **1988**, *38*, 11337.
(13) McCabe, E. E.; Greaves, C. *J. Fluorine Chem.* **2007**, *128*, 448.
(14) Greaves, C.; Francesconi, M. G. *Curr. Opin. Solid State Mater. Sci.* **1998**, *3*, 132.
(15) Aikens, L. D.; Gillie, L. J.; Li, R. K.; Greaves, C. *J. Mater. Chem.* **2002**, *12*, 264.
(16) Sivakumar, T.; Wiley, J. B. *Mater. Res. Bull.* **2009**, *44*, 74.
(17) Slater, P. R.; Hodges, J. P.; Francesconi, M. G.; Edwards, P. P.; Greaves, C.; Gameson, I.; Slaski, M. *Physica C* **1995**, *253*, 16.
(18) Battle, P. D.; Bollen, S. K.; Powell, A. V. *J. Solid State Chem.* **1992**, *99*, 267.
(19) Gallon, D. J.; Battle, P. D.; Blundell, S. J.; Burley, J. C.; Coldea, A. I.; Cussen, E. J.; Rosseinsky, M. J.; Steer, C. *Chem. Mater.* **2002**, *14*, 3976.
(20) Larson, A. C.; Von Dreele, R. B. *Los Alamos National Laboratory Report LAUR* **2000**, 86−748.
(21) Case, G. S.; Hector, A. L.; Levason, W.; Needs, R. L.; Thomas, M. F.; Weller, M. T. *J. Mater. Chem.* **1999**, *9*, 2821.
(22) Greenhalgh, R.; Riley, J. P. *Anal. Chim. Acta* **1961**, *25*, 179.
(23) Sears, V. F. *Neutron News* **1992**, *3*, 26.
(24) Brese, N. E.; O'Keeffee, M. *Acta Crystallogr., Sect. B: Struct. Sci.* **1991**, *B47*, 192.
(25) Greis, O.; Petzel, T. Z. *Anorg. Allg. Chem.* **1974**, *403*, 1.
(26) Takeda, T.; Nagata, M.; Kobayashi, H.; Kanno, R.; Kawamoto, Y.; Takano, M. *J. Solid State Chem.* **1998**, *140*, 182.
(27) Renard, C.; Daviero-Minaud, S.; Abraham, F. *J. Solid State Chem.* **1999**, *143*, 266.

(28) Fischer, D.; Hoppe, R.; Mogare, K. M.; Jansen, M. *Z. Naturforsch., B: Chem. Sci.* **2005**, *60*, 1113.
(29) Shikano, M.; Kremer, R. K.; Ahrens, M.; Koo, H. J.; Whangbo, M. H.; Darriet, J. *Inorg. Chem.* **2004**, *43*, 5.
(30) Mugavero, S. J.; Gemmill, W. R.; Roof, I. P.; zur Loye, H. C. *J. Solid State Chem.* **2009**, *182*, 1950.
(31) Battle, P. D.; Goodenough, J. B.; Price, R. *J. Solid State Chem.* **1983**, *46*, 234.
(32) Dass, R. I.; Yan, J. Q.; Goodenough, J. B. *Phys. Rev. B* **2004**, 69.
(33) Goodenough, J. B. *Magnetism and the Chemical Bond*; Wiley: New York, 1963.